

**Research note**

**Inverse propagation in 1.5-dimensional amplitude-versus-offset joint migration inversion**

Sun, Yimin; Verschuur, Eric

**DOI**

[10.1111/1365-2478.13144](https://doi.org/10.1111/1365-2478.13144)

**Publication date**

2021

**Document Version**

Accepted author manuscript

**Published in**

Geophysical Prospecting

**Citation (APA)**

Sun, Y., & Verschuur, E. (2021). Research note: Inverse propagation in 1.5-dimensional amplitude-versus-offset joint migration inversion. *Geophysical Prospecting*, 70(1), 222-234. <https://doi.org/10.1111/1365-2478.13144>

**Important note**

To cite this publication, please use the final published version (if applicable). Please check the document version above.

**Copyright**

Other than for strictly personal use, it is not permitted to download, forward or distribute the text or part of it, without the consent of the author(s) and/or copyright holder(s), unless the work is under an open content license such as Creative Commons.

**Takedown policy**

Please contact us and provide details if you believe this document breaches copyrights. We will remove access to the work immediately and investigate your claim.

# **Research Note: Inverse Propagation in 1.5-Dimensional Amplitude-versus-Offset Joint Migration Inversion**

Yimin Sun<sup>1,\*</sup> and Eric Verschuur<sup>2</sup>

<sup>1</sup>Aramco Research Center - Delft, Aramco Europe, Delft, 2628 ZD, The Netherlands.

<sup>2</sup>Delft University of Technology, Delft, 2600 GA, The Netherlands

\*Correspondence email: [sun.delft@gmail.com](mailto:sun.delft@gmail.com)

## **ABSTRACT**

The state-of-the-art joint migration inversion faces the so-called amplitude-versus-offset challenge, due to adopting over-simplified one-way propagation, reflection and transmission operators to avoid over-parameterization in the inversion process. To overcome this challenge, we apply joint migration inversion to horizontally layered media (or 1.5-dimensional media) and parameterize the solution space via density and velocity models. In this scenario, one-way propagation, reflection and transmission operators required by the joint migration inversion process can be analytically and correctly derived from the subsurface models, so the amplitude-versus-offset challenge is successfully overcome. We introduce a new concept, which is named ‘inverse propagation’, into our 1.5-dimensional amplitude-versus-offset joint migration inversion. It can correctly reconstruct subsurface wavefields by using a surface-recorded receiver wavefield with all the influence of transmission, reflection and multiples accounted for. A synthetic example is used to demonstrate the correctness of the inverse propagation. This work is the foundation to further develop the 1.5-dimensional amplitude-versus-offset joint migration inversion technology.

**KEYWORDS**

Joint Migration Inversion, Inverse Propagation

## Introduction

As a relatively new technology, joint migration inversion (JMI) is formulated in the acoustic framework and simultaneously deals with velocity model building and seismic imaging (Berkhout, 2014b). JMI belongs to the school of full waveform inversion (FWI), and it tries to fit forward modeled data with measurements (Verschuur et al., 2016). Many similarities can be found between JMI and imaging-oriented FWI (Kalinicheva et al., 2020; Zhang et al., 2020), reflection FWI (Xu et al., 2013; Valensi et al., 2017; Gisolf et al., 2021) and migration based travelttime waveform inversion (Clément et al., 2001; Chavent, 2017). JMI aims at exploiting all multiples in data for inversion, and the key is in its unique modeling engine, which is named full wavefield modeling (FWMod) (Berkhout, 2014a). JMI and FWMod are based upon wavefield separation (Sun and Fei, 2018; Sun and Fei, 2020), and the concrete wavefield separation scheme adopted therein is based on Bremmer's series using one-way operators (Berkhout, 2014a). JMI parameterizes the subsurface via a migration velocity model and a reflectivity model. Furthermore, it assumes that these two models are decoupled (Berkhout, 2014b; Sun et al., 2020). Although in physics a reflectivity model should be dependent on propagation angles, this in reality creates an enormous solution space for inversion in JMI, which leads to over-parametrization of the inverse problem where many velocity models with suitable angle-dependent reflectivities can fit the data. Consequently, current implementations of JMI adopt over-simplified operators (Sun et al., 2018b): for propagation operators, it uses the local explicit operators (Etgen, 1994); for transmission and reflection operators, it uses angle-independent operators (Verschuur et al., 2016; Sun et al., 2019). Via a comparison study, we have systematically investigated the influence of these simplified operators on JMI results (Sun et al. 2020), where the amplitude-versus-offset (AVO) challenge has been pointed out for the current JMI. Some initiatives to overcome this AVO challenge for JMI are currently underway (Davydenko and Verschuur, 2017; Qu et al., 2018; Sun and Verschuur, 2020).

In this paper, we propose to apply acoustic JMI to horizontally layered media, which is also commonly named 1.5-dimensional media. Although we still use one-way propagation, reflection and transmission operators to describe wave propagations, we now first parameterize the solution space via a velocity model and a density model, and next use these models to derive all those one-way operators required by JMI. In such a scenario, one-way propagation, reflection and transmission operators can be analytically defined in a physically correct way (Berkhout, 1987), so we naturally overcome the AVO challenge. To avoid confusions, throughout the rest of this paper, we refer to our new variant of JMI by 1.5D-AVO-JMI, and refer to the current JMI technology (Berkhout, 2014b) by the traditional JMI. 1.5D-AVO-JMI should have applications in locally horizontally layered media containing strong multiple generators. We further introduce a new concept named ‘inverse propagation’, which can correctly reconstruct subsurface wavefields required by 1.5D-AVO-JMI using a surface-recorded receiver wavefield and accommodating physical causality effects during the course of wave propagation.

The rest of this paper is organized as follows. We first formulate a detailed theory of 1.5D-AVO-FWMod, which is the modeling engine used in 1.5D-AVO-JMI. We next introduce the ‘inverse propagation’ concept in detail. We further discuss how we deal with the challenge of numerical instability when applying the inverse propagation in reality, and use a synthetic example to demonstrate the correctness of the ‘inverse propagation’ concept.

### **1.5-Dimensional Amplitude-versus-Offset Full Wavefield Modeling**

Our theories for both 1.5D-AVO-FWMod and 1.5D-AVO-JMI are derived in the temporal frequency – spatial wavenumber (FK) domain. We consider a pressure signal corresponding to a combination of  $k_x$  and  $\omega$ , where  $k_x$  is a spatial wavenumber in the x direction and  $\omega$  is an angular frequency. Our theories are acoustic, and thus the 1.5D media are isotropic. Under these considerations, we can set spatial wavenumbers in the y direction to zeroes, i.e.,  $k_y = 0$ , as long as we make sure to have sufficient

sampling for  $k_x$ . As a result, for a temporal frequency  $f$  and a medium with a velocity  $c$ , the relationships connecting spatial wavenumbers  $k_x$  and  $k_z$  with a corresponding wavenumber  $k$  are:

$$\omega = 2\pi f, \quad k = \frac{\omega}{c}, \quad k_x^2 + k_z^2 = k^2. \quad (1)$$

The wavefield propagation model in both 1.5D-AVO-FWMod and 1.5D-AVO-JMI is shown in Figure 1, which is similar to that in the traditional JMI (Sun et al., 2019). Please note that all the wavefield-related symbols in Figure 1 are actually scalars subject to a certain combination of  $k_x$  and  $\omega$ , as there exist no physically non-linear effects, such as frequency conversion, in our wavefield propagation theory. In other words, both the spatial and the temporal frequencies are decoupled, and thus wave propagation equations can be written independently for different combinations of  $k_x$  and  $\omega$ . For example,  $q^+(z_m)$  there actually represents  $q^+(z_m; k_x, \omega)$ . The symbols shown in Figure 1 are defined as follows:  $\rho$  and  $c$  are velocity and density of a layer, the superscript  $+$  or  $-$  represents down-going or up-going propagation,  $z_m$  is the depth of the  $m^{\text{th}}$  interface in the  $z$  direction,  $p$  is an incoming wavefield,  $q$  is an outgoing wavefield,  $t$  or  $r$  is a transmission or reflection coefficient,  $s$  is an injection source wavefield, and  $w$  is a one-way propagator. In 1.5D media,  $w(z_m, z_{m+1})$  and  $r^-(z_m)$  have been discussed before (Berkhout, 1987; Sun et al., 2018a), and they can be written as:

$$w(z_{m+1}, z_m) = \begin{cases} \exp(-i \cdot k_{z,m} \cdot |z_{m+1} - z_m|) & \text{if } k_m^2 \geq k_x^2 \\ \exp(-|k_{z,m}| \cdot |z_{m+1} - z_m|) & \text{otherwise} \end{cases}, \quad (2)$$

$$r^-(z_m) = \frac{\rho_{m+1} \cdot k_{z,m} - \rho_m \cdot k_{z,m+1}}{\rho_{m+1} \cdot k_{z,m} + \rho_m \cdot k_{z,m+1}}, \quad (3)$$

$$k_{z,m} = \sqrt{k_m^2 - k_x^2}, \quad (4)$$

where  $k_m = \frac{\omega}{c_m}$ .

Similar to FWMod, 1.5D-AVO-FWMod also engages iterations in its modeling process, and we use  $n$  to explicitly denote its modeling iteration:  $n=0$  is the first iteration corresponding to primaries;  $n=1$  is the

second iteration corresponding to the first-order multiples; ... Using symbols shown in Figure 1, the theory of 1.5D-AVO-FWMod can be formulated as below:

$$q_n^+(z_m) = s^+(z_m) + t^+(z_m) \cdot p_n^+(z_m) + r^+(z_m) \cdot p_{n-1}^-(z_m), \quad (5)$$

$$q_n^-(z_m) = s^-(z_m) + t^-(z_m) \cdot p_n^-(z_m) + r^-(z_m) \cdot p_n^+(z_m), \quad (6)$$

$$p_n^+(z_m) = w(z_m, z_{m-1}) \cdot q_n^+(z_{m-1}), \quad (7)$$

$$p_n^-(z_m) = w(z_m, z_{m+1}) \cdot q_n^-(z_{m+1}), \quad (8)$$

$$r^-(z_m) = -r^+(z_m), \quad (9)$$

$$t^+(z_m) = 1 + r^-(z_m), \quad (10)$$

$$t^-(z_m) = 1 + r^+(z_m), \quad (11)$$

$$w(z_m, z_{m+1}) = w(z_{m+1}, z_m), \quad (12)$$

where  $n$  is the multiple order (or the iteration order). Note that  $p_{-1}^-(z_m) = 0$  in equation (5).

Equations (1) through (12) reflect the philosophy behind Bremmer's series. Each iteration of 1.5D-AVO-FWMod corresponds to one order of multiples, and it comprises a wavefield propagating from the surface of model to the bottom reflection interface of model and then being reflected back to the surface. During the course of one iteration, transmission and reflection effects are accounted for, and contributions from previous iterations, i.e., multiples, are also accommodated. Inclusion of surface-related multiples can be explicitly controlled by  $q_n^+(z_0)$ , which is the down-going and out-going wavefield at the surface:

$$q_n^+(z_0) = \begin{cases} s^+(z_0) + r^+(z_0) \cdot p_{n-1}^-(z_0), & \text{free surface} \\ s^+(z_0), & \text{absorption surface} \end{cases} \quad (13)$$

Although the theory of 1.5D-AVO-FWMod looks similar to that of FWMod (Berkhout, 2014a; Sun et al., 2019) in its formality, there exist fundamental differences:

- The solution space is parameterized via medium parameters  $\rho$  and  $c$ .
- Transmission and reflection effects can now be physically accounted for via equations (3), (9)~(11), and hence the AVO effect in input data can be correctly simulated.

- All components are separable in the  $(k_x, \omega)$  domain, and hence we are now dealing with scalar computations. In other words, all symbols in the equations (5)~(12) are scalars.

In seismic data acquisition, usually sources are located at the surface. Furthermore, we normally estimate a source wavefield that only contains downward propagating components. So throughout this paper, we set the below requirements to the source terms in equations (5) and (6):

$$s^-(z_m) = 0 \text{ for all } z_m, \quad (14)$$

$$s^+(z_m) = 0 \text{ for } z_m \neq z_0. \quad (15)$$

Note the traditional JMI (Berkhout, 2014b; Verschuur et al., 2016; Sun et al., 2019; Sun et al., 2020) adopts conditions similar to equations (14) and (15).

## **Inverse Propagation in 1.5-Dimensional Amplitude-versus-Offset Joint Migration Inversion**

In the traditional JMI, a crucial component is to use a receiver wavefield recorded at the surface to reconstruct proper subsurface wavefields for the purpose of gradient calculations. Reconstructing subsurface wavefields is not a trivial task as it is highly nonlinear and engages effects of physical causality. The backward propagation scheme is the engine for reconstructing these subsurface wavefields in the traditional JMI, but this scheme only considers dealing with the propagation effect and the transmission effect (Staal, 2015; Sun et al., 2019). We hereby propose a new concept that is named ‘inverse propagation’ for surface-recorded receiver wavefields. It aims at correctly addressing the effects of propagation, transmission, reflection and physical causality to reconstruct proper subsurface wavefields from a surface receiver wavefield for 1.5D-AVO-JMI.

In order to understand why we introduce this new concept of inverse propagation to 1.5D-AVO-JMI, we use a 2-layer model, shown in Figure 2, to demonstrate the limitations of the backward propagation

scheme used in the traditional JMI. We first use the primaries, i.e., the 1<sup>st</sup> iteration of 1.5D-AVO-FWMod, as an example, and its complete simulation process is as follows:

$$q_0^+(z_0) = s^+(z_0), \quad (16)$$

$$p_0^+(z_1) = w(z_1, z_0) \cdot q_0^+(z_0), \quad (17)$$

$$q_0^+(z_1) = t^+(z_1) \cdot p_0^+(z_1), \quad (18)$$

$$p_0^+(z_2) = w(z_2, z_1) \cdot q_0^+(z_1), \quad (19)$$

$$q_0^-(z_2) = r^-(z_2) \cdot p_0^+(z_2), \quad (20)$$

$$p_0^-(z_1) = w(z_1, z_2) \cdot q_0^-(z_2), \quad (21)$$

$$q_0^-(z_1) = t^-(z_1) \cdot p_0^-(z_1) + r^-(z_1) \cdot p_0^+(z_1), \quad (22)$$

$$p_0^-(z_0) = w(z_0, z_1) \cdot q_0^-(z_1). \quad (23)$$

Please note that all symbols in equations (16) through (23) are scalars, as already discussed in the previous section.

Starting with the surface recorded wavefield  $p_0^-(z_0)$ , the backward propagation scheme (Staal, 2015; Sun et al., 2019) reconstructs the wavefields  $\widetilde{q}_0^-(z_1)$  and  $\widetilde{p}_0^-(z_1)$  as follows:

$$\widetilde{q}_0^-(z_1) = w(z_0, z_1)^{-1} \cdot p_0^-(z_0) = w(z_0, z_1)^{-1} \cdot w(z_0, z_1) \cdot q_0^-(z_1) = q_0^-(z_1), \quad (24)$$

$$\begin{aligned} \widetilde{p}_0^-(z_1) &= t^-(z_1)^{-1} \cdot \widetilde{q}_0^-(z_1) = t^-(z_1)^{-1} \cdot [t^-(z_1) \cdot p_0^-(z_1) + r^-(z_1) \cdot p_0^+(z_1)] \\ &= p_0^-(z_1) + t^-(z_1)^{-1} \cdot r^-(z_1) \cdot p_0^+(z_1). \end{aligned} \quad (25)$$

Comparing equations (24) and (25) to equations (22) and (21), we can clearly see that although the backward propagation scheme in the traditional JMI can correctly deal with the propagation effect, it violates the causality of forward wavefield propagation by incorrectly introducing the term  $t^-(z_1)^{-1} \cdot r^-(z_1) \cdot p_0^+(z_1)$  into the reconstructed wavefield  $\widetilde{p}_0^-(z_1)$ .

We next use a total wavefield containing both primaries and the first order of multiples, i.e., to run 2 iterations of 1.5D-AVO-FWMod, from this 2-layer model to further demonstrate this causality effect in

the backward propagation scheme of the traditional JMI. Iteration 2 of 1.5D-AVO-FWMod follows equations (16) through (23) as shown below:

$$q_1^+(z_0) = s^+(z_0) + r^+(z_0) \cdot p_0^-(z_0), \quad (26)$$

$$p_1^+(z_1) = w(z_1, z_0) \cdot q_1^+(z_0), \quad (27)$$

$$q_1^+(z_1) = t^+(z_1) \cdot p_1^+(z_1) + r^+(z_1) \cdot p_0^-(z_1), \quad (28)$$

$$p_1^+(z_2) = w(z_2, z_1) \cdot q_1^+(z_1), \quad (29)$$

$$q_1^-(z_2) = r^-(z_2) \cdot p_1^+(z_2), \quad (30)$$

$$p_1^-(z_1) = w(z_1, z_2) \cdot q_1^-(z_2), \quad (31)$$

$$q_1^-(z_1) = t^-(z_1) \cdot p_1^-(z_1) + r^-(z_1) \cdot p_1^+(z_1), \quad (32)$$

$$p_1^-(z_0) = w(z_0, z_1) \cdot q_1^-(z_1). \quad (33)$$

If we use the backward propagation scheme in the traditional JMI with the measured surface wavefield  $p_1^-(z_0)$ , i.e., equation (33), we can get the reconstructed wavefields  $\widetilde{q}_1^-(z_1)$  and  $\widetilde{p}_1^-(z_1)$  as follows:

$$\widetilde{q}_1^-(z_1) = w(z_0, z_1)^{-1} \cdot p_1^-(z_0) = w(z_0, z_1)^{-1} \cdot w(z_0, z_1) \cdot q_1^-(z_1) = q_1^-(z_1), \quad (34)$$

$$\begin{aligned} \widetilde{p}_1^-(z_1) &= t^-(z_1)^{-1} \cdot \widetilde{q}_1^-(z_1) = t^-(z_1)^{-1} \cdot [t^-(z_1) \cdot p_1^-(z_1) + r^-(z_1) \cdot p_1^+(z_1)] \\ &= p_1^-(z_1) + t^-(z_1)^{-1} \cdot r^-(z_1) \cdot p_1^+(z_1). \end{aligned} \quad (35)$$

Similar to the conclusions reached about equations (24) and (25), we can see that although the backward propagation scheme can correctly deal with the propagation effect, it violates the causality by incorrectly introducing the term  $t^-(z_1)^{-1} \cdot r^-(z_1) \cdot p_1^+(z_1)$  into the reconstructed wavefield  $\widetilde{p}_1^-(z_1)$ .

We now introduce the inverse propagation scheme, which can correctly account for this causality influence, in a general situation. We first consider reconstructing up-going wavefields from a surface receiver wavefield  $p_n^-(z_0)$ . According to equation (8), the up-going and out-going wavefield  $\widetilde{q}_n^-(z_m)$  can be computed as

$$\widetilde{q}_n^-(z_m) = w(z_{m-1}, z_m)^{-1} \cdot \widetilde{p}_n^-(z_{m-1}), \quad (36)$$

where  $\widetilde{p}_{l,n}^-(z_{m-1})$  is the reconstructed up-going and incoming wavefield at  $z = z_{m-1}$ .

At the surface, i.e.  $z = z_0$ , we have a particular relationship for the  $\widetilde{p}_n^-(z_0)$ :

$$\widetilde{p}_n^-(z_0) = p_n^-(z_0). \quad (37)$$

According to the equations (6), (14) and (15),  $\widetilde{p}_n^-(z_m)$  where  $m > 0$  can be reconstructed by

$$\widetilde{p}_n^-(z_m) = t^-(z_m)^{-1} \cdot \widetilde{q}_n^-(z_m) - t^-(z_m)^{-1} \cdot r^-(z_m) \cdot p_n^+(z_m), \quad (38)$$

where the term  $p_n^+(z_m)$  is obtained via a forward simulation using 1.5D-AVO-FWMod, i.e., through the equations (1)~(13) with a source wavefield and subsurface models provided by users as the input. We name the term ‘ $-t^-(z_m)^{-1} \cdot r^-(z_m) \cdot p_n^+(z_m)$ ’ a compensation term. It bears the causality effect on the reconstruction of  $\widetilde{p}_n^-(z_m)$  from the surface wavefield  $p_n^-(z_0)$ , and it has to be accounted for in order to correctly reconstruct  $\widetilde{p}_n^-(z_m)$ . Although the traditional JMI ignores this causality effect in its backward propagation scheme (Berkhout, 2014b; Verschuur et al., 2016; Sun et al., 2019; Sun et al., 2020), this compensation term now is a key component in the inverse propagation scheme of 1.5D-AVO-JMI. Please note that Berkhout (2014a) does describe a different way of inverse full wavefield modeling, which is via subtraction of the scattering term at each depth level. However, this cannot provide a direct estimate of the upgoing wavefield as shown in eq. (38).

At the bottom reflection interface, i.e.,  $z = z_{max}$ , according to equation (6), we can retrieve the inversely propagated down-going and incoming wavefield  $\widetilde{p}_n^+(z_m)$  by

$$\widetilde{p}_n^+(z_{max}) = r^-(z_{max})^{-1} \cdot \widetilde{q}_n^+(z_{max}). \quad (39)$$

Note here we adopt the condition  $p_n^-(z_{max}) = 0$ , as we are now considering the bottom reflection interface.

With  $\widetilde{p}_n^+(z_{max})$  being available from equation (39), we can further recursively reconstruct the down-going and outgoing (or incoming) wavefield  $\widetilde{q}_n^+(z_m)$  (or  $\widetilde{p}_n^+(z_m)$ ). According to equations (7) and (5), they can be calculated as:

$$\widetilde{q}_n^+(z_m) = w(z_{m+1}, z_m)^{-1} \cdot \widetilde{p}_n^+(z_{m+1}), \quad (40)$$

$$\widetilde{p}_n^+(z_m) = t^+(z_m)^{-1} \cdot \widetilde{q}_n^+(z_m) - t^+(z_m)^{-1} \cdot r^+(z_m) \cdot p_{n-1}^-(z_m). \quad (41)$$

Similar to the equation (38), the term ‘ $-t^+(z_m)^{-1} \cdot r^+(z_m) \cdot p_{n-1}^-(z_m)$ ’ is also a compensation term addressing the causality effect, and  $p_{n-1}^-(z_m)$  has to be obtained via a forward simulation using 1.5D-AVO-FWMod.

The equations (36) through (41) form the complete theory of inverse propagation in 1.5D-AVO-JMI. Via the compensation terms, the inverse propagation correctly accounts for the influence of propagation, transmission, reflection and multiples to reconstruct subsurface wavefields using a surface receiver wavefield. However, in order to obtain the compensation terms, we need to run 1.5D-AVO-FWMod for the required  $p_n^+(z_m)$  and  $p_{n-1}^-(z_m)$  in the equations (38) and (41).

Before wrapping up this section, we would like to emphasize again that our inverse propagation scheme differs from the backward propagation scheme in the traditional JMI in the compensation terms. The compensation terms reflect causality, and they account for influences of transmission, reflection and multiples.

## Discussion

The inverse propagation introduced above, i.e., the equations (36) through (41), is a recursive process, and it engages many inverse calculations, including  $w(z_{m+1}, z_m)^{-1}$ ,  $t^-(z_m)^{-1}$ ,  $t^+(z_m)^{-1}$  and  $r^-(z_{max})^{-1}$ . Note all these symbols are scalars in 1.5D-AVO-JMI, as already explained earlier in this paper. In practice, this poses a severe challenge for the numerical stability. As far as we know, there are two ways to overcome this challenge. The first way is to resort to high-precision arithmetic libraries, for instance Multiple Precision Toolbox for MATLAB (Barrowes, 2020) and The GNU MPFR Library

(Fousse et al., 2005). The other way, which we believe is a more practical solution and thus is adopted in this paper, is a phase-guided solution. Details of this phase-guided algorithm can be found in Oppenheim and Lim (1981) and Bakulin et al. (2020). In this discussion section, we briefly introduce how we use this algorithm to stabilize our numerical calculations in the inverse propagation scheme.

As introduced above, in the inverse propagation of 1.5D-AVO-JMI, we need to do forward simulation to get  $p_n^+(z_m)$  and  $p_{n-1}^-(z_m)$  for compensation terms. To stabilize the calculation, we also use the corresponding forward-simulated wavefield amplitudes as the amplitudes of reconstructed wavefields. In other words, in our example, equations (36) through (41) are implemented as follows:

$$\widetilde{q}_n^-(z_m) = w(z_{m-1}, z_m)^{-1} \cdot \widetilde{p}_n^-(z_{m-1}) \cdot |w(z_{m-1}, z_m)^{-1} \cdot \widetilde{p}_n^-(z_{m-1})|^{-1} \cdot |q_n^-(z_m)|, \quad (42)$$

$$\begin{aligned} \widetilde{p}_n^-(z_m) = [t^-(z_m)^{-1} \cdot \widetilde{q}_n^-(z_m) - t^-(z_m)^{-1} \cdot r^-(z_m) \cdot p_n^+(z_m)] \\ \cdot |t^-(z_m)^{-1} \cdot \widetilde{q}_n^-(z_m) - t^-(z_m)^{-1} \cdot r^-(z_m) \cdot p_n^+(z_m)|^{-1} \cdot |p_n^-(z_m)|, \end{aligned} \quad (43)$$

$$\widetilde{p}_n^+(z_{max}) = r^-(z_{max})^{-1} \cdot \widetilde{q}_n^-(z_{max}) \cdot |r^-(z_{max})^{-1} \cdot \widetilde{q}_n^-(z_{max})|^{-1} \cdot |p_n^+(z_{max})|, \quad (44)$$

$$\widetilde{q}_n^+(z_m) = w(z_{m+1}, z_m)^{-1} \cdot \widetilde{p}_n^+(z_{m+1}) \cdot |w(z_{m+1}, z_m)^{-1} \cdot \widetilde{p}_n^+(z_{m+1})|^{-1} \cdot |q_n^+(z_m)|, \quad (45)$$

$$\begin{aligned} \widetilde{p}_n^+(z_m) = [t^+(z_m)^{-1} \cdot \widetilde{q}_n^+(z_m) - t^+(z_m)^{-1} \cdot r^+(z_m) \cdot p_{n-1}^-(z_m)] \\ \cdot |t^+(z_m)^{-1} \cdot \widetilde{q}_n^+(z_m) - t^+(z_m)^{-1} \cdot r^+(z_m) \cdot p_{n-1}^-(z_m)|^{-1} \cdot |p_n^+(z_m)|, \end{aligned} \quad (46)$$

where  $|a|$  means taking the amplitude of the input variable  $a$ . Note that all demonstrations in the Example section use the equations (42) through (46) for the inverse propagation.

Before wrapping up this section, we would like to point out that our phase-guided solution requires a good estimation of the input source wavelet for forward simulation. Detailed discussion on retrieving a high-fidelity source wavelet from raw seismic data is beyond the scope of this paper, and interested readers can refer to Verschuur et al. (1989), Carvalho and Weglein (1994) and Matson (2000) for some technical details.

## Example

We use a 1.5D synthetic model, shown in Figure 3, to demonstrate the inverse propagation scheme in 1.5D-AVO-JMI. There exist several multiple generators in the subsurface. The source wavefield  $s^+(z_0)$  in our demo is shown in Figure 4 in both the FK domain and the x-t domain. Our source wavefield covers a spectrum between 0.2 Hz and 30 Hz. As the purpose of this paper is to demonstrate the inverse propagation concept in 1.5D-AVO-JMI, the source wavefield is our a-priori knowledge. We use the 1.5D-AVO-FWMod as our forward modeling engine, and the data simulation related parameters in our example are as follows: both the initial frequency and the frequency step are 0.2 Hz, and the maximum frequency is 30 Hz; the maximum source-receiver offset is 5 km, and the receiver spacing is 25 m; the grid size in the z direction is 5 m.

Figure 5 shows the surface wavefield when only internal multiples are considered in our data, i.e., with an absorption surface condition applied. We set the maximum order of internal multiples to 10. Via the inverse propagation scheme, i.e., the equations (36) through (41) and using the models and the source wavefield shown in Figures 3 and 4 as the input, we reconstruct the up-going and incoming wavefield  $\widetilde{p}_n^-$  at  $z = 175 \text{ m}$ , the down-going and incoming wavefield  $\widetilde{p}_n^+$  at  $z = 125 \text{ m}$ , and the down-going and outgoing wavefield  $\widetilde{q}_{n-1}^+$  at the surface. Our reconstructed wavefields are shown in the top middle pictures in Figures 6, 7 and 8; the top left pictures in those figures show the ground truth; the top right pictures show the reconstructed wavefields by the backward propagation scheme in the traditional JMI (we use OJMI to represent this scheme on a figure); the bottom middle pictures show the difference between the ground truth and the reconstructed wavefields by the inverse propagation; the bottom right pictures show the difference between the ground truth and the reconstructed wavefields by the backward propagation. We can easily observe that our inverse propagation scheme indeed correctly reconstructs all subsurface wavefields when the input models and the source wavefield are correct, while the backward propagation scheme yields inaccuracies. Figure 9 shows the surface wavefield when both surface and

internal multiples are considered in our data, i.e., with a free surface condition applied. We set the maximum order of multiples to 5 in this example. Comprehensive result comparisons, the same to those shown in Figures 6, 7 and 8, are shown in Figures 10, 11 and 12. In this situation, we can also easily observe that our inverse propagation scheme works correctly when the input models and the source wavefield are correct.

## **Conclusions**

In this paper, we introduce the inverse propagation concept in the 1.5-dimensional amplitude-versus-offset joint migration inversion (1.5D-AVO-JMI). 1.5D-AVO-JMI still uses one-way propagation, transmission and reflection operators to describe wave propagation, but it first parameterizes the subsurface via a density model and a velocity model and then uses these models to derive the corresponding physical one-way operators. 1.5D-AVO-JMI overcomes the amplitude-versus-offset challenge as now one-way propagation, reflection and transmission operators are physically correct. The inverse propagation concept uses the compensation terms to account for causality effects during the course of wavefield propagation, and it is a theoretically rigorous way to reconstruct subsurface wavefields in 1.5D-AVO-JMI. We also discuss a practical challenge when implementing the inverse propagation in 1.5D-AVO-JMI, which is the numerical stability, and we propose to use the phase-guided algorithm to overcome it. Our synthetic examples corroborate the correctness of our theories. We believe this work can act as the solid theoretical foundation to further develop the 1.5D-AVO-JMI technology.

## REFERENCES

- Bakulin, A., I. Silvestrov and D. Neklyudov, 2020. Importance of phase guides from beamformed data for processing multi-channel data in highly scattering media, *The Journal of the Acoustical Society of America*, 147 (6), EL447-EL452.
- Barrowes, B., 2020. Multiple Precision Toolbox for MATLAB (<https://www.mathworks.com/matlabcentral/fileexchange/6446-multiple-precision-toolbox-for-matlab>), MATLAB Central File Exchange. Retrieved September 10, 2020.
- Berkhout, A. J., 1987. *Applied seismic wave theory*, Volume 1: Elsevier.
- Berkhout, A. J., 2014a. Review Paper: An outlook on the future of seismic imaging, Part I: forward and reverse modelling: *Geophysical Prospecting*, 62, 911-930.
- Berkhout, A. J., 2014b. Review Paper: An outlook on the future of seismic imaging, Part III: Joint Migration Inversion: *Geophysical Prospecting*, 62, 950-971.
- Carvalho, P. M. and A. B. Weglein, 1994. Wavelet estimation for surface multiple attenuation using a simulated annealing algorithm: *SEG Expanded Abstracts*, 1481-1484.
- Clément, F., G. Chavent, and S. Gómez, 2001. Migration-based traveltime waveform inversion of 2-D simple structures: A synthetic example: *Geophysics*, 66, 845-860.
- Chavent, G., 2017. Data space reflectivity and the migration based travel time approach to FWI: *EAGE Extended Abstracts*, WS09 A01.
- Davydenko, M. and D. J. Verschuur, 2017, Full-wavefield estimation of angle-dependent reflectivity and migration velocity: *SEG Technical Program Expanded Abstracts*, 5631-5635.
- Etgen, J. T., 1994. Stability of explicit depth extrapolation through laterally-varying media: *SEG Expanded Abstracts*, 1266-1269.
- Fousse, L., G. Hanrot, V. Lefèvre, P. Pélissier, P. Zimmermann, 2005. MPFR: A Multiple-Precision Binary Floating Point Library With Correct Rounding, Research Report, RR-5753, INRIA, pp. 15, inria-00070266.

- Kalinicheva, T., M. Warner, and F. Mancini, 2020. Full-bandwidth FWI: SEG Expanded Abstracts, 651-655.
- Gisolf, A., P. R. Haffinger, P. Doulgeris, 2021. AVO modeling and interpretation with the help of the 1.5D elastic wave-equation: *First Break*, 39(3), 93-100.
- Matson, K., 2000. An overview of wavelet estimation using free-surface multiple removal: *The Leading Edge*, 19 (1), 50-55.
- Oppenheim, A. V. and J. S. Lim, 1981. The importance of phase in signals, *Proc. IEEE*, 69, 529-541.
- Qu, Sh., Y. Sun and E. Verschuur, 2018. Mitigating amplitude versus ray-parameter effect in joint migration inversion using a zero-lag cross-correlation objective function of redatumed wavefields: SEG Technical Program Expanded Abstracts, 1133-1137.
- Staal, X., 2015, Combined imaging and velocity estimation by Joint Migration Inversion: Ph.D. thesis, Delft University of Technology, <https://repository.tudelft.nl/islandora/object/uuid:f9cfa765-dac4-4954-9b6b-01b8c7345018/?collection=research> .
- Sun, Y., E. Verschuur and R. van Borselen, 2018a. Acoustic propagation operators for pressure signals on an arbitrarily curved surface in a homogeneous medium: *Journal of Applied Geophysics*, 150, 314-324.
- Sun, Y., Y. S. Kim, Sh. Qu, E. Verschuur, A. Almomin and R. van Borselen, 2018b. Joint migration inversion versus FWI-RTM: a comparison study on a 2D realistic deep water model: EAGE Extended Abstract, Th P3 10.
- Sun, Y. and T. W. Fei, 2018. Wavefield separation at an arbitrary propagation direction via FK filtering: SEG Expanded Abstracts, 4171-4175.
- Sun, Y., E. Verschuur and Sh. Qu, 2019. Research note: Derivations of gradients in angle-independent joint migration inversion: *Geophysical Prospecting*, 67, 572-579.
- Sun, Y., Y. S. Kim, Sh. Qu and E. Verschuur, 2020. Joint Migration Inversion: features and challenges: *The Journal of Geophysics and Engineering*, 17 (3), 525-538.
- Sun, Y. and T. W. Fei, 2020. Flank-preserving de-primary reverse time migration: *Geophysics*, accepted.

- Sun, Y. and E. Verschuur, 2020. Full wavefield modelling using rigorous one-way propagation, reflection and transmission operators: SEG Expanded Abstracts, 2694-2698.
- Valensi, R., R. Baina and V. Duprat, 2017, Reflection waveform inversion method: solutions to the reflectivity-background coupling problem and consequences on the convergence: 79<sup>th</sup> Ann. Internat. Mtg., EAGE, Expanded abstracts, WS09 D03.
- Verschuur, D. J., A. J. Berkhout, and C. P. A. Wapenaar, 1989. Wavelet estimation by prestack multiple elimination: SEG Expanded Abstracts, 1129-1132.
- Verschuur, D. J., X. R. Staal, and A. J. Berkhout, 2016, Joint migration inversion: Simultaneous determination of velocity fields and depth images using all orders of scattering: The Leading Edge, **35**, 1037-1046.
- Xu, Sh., F. Chen, G. Lambaré, and Y. Zhang, 2013. Full waveform inversion of reflected seismic data: Journal of Seismic Exploration, 22 (5), 449-462.
- Zhang, Zh., Z. Wu, Zh. Wei, J. Mei, R. Huang, and P. Wang, 2020. FWI Imaging: Full-wavefield imaging through full-waveform inversion: SEG Expanded Abstracts, 656-660.

## LIST OF FIGURES

Figure 1: The fundamental wavefield propagation model used in 1.5D-AVO-FWMod and 1.5D-AVO-JMI. Note that all the wavefield-related symbols in this figure are actually subject to a certain combination of  $k_x$  and  $\omega$ . For example,  $q^+(z_m)$  there actually represents  $q^+(z_m; k_x, \omega)$ . The symbols shown in this figure are defined as follows:  $\rho$  and  $c$  are velocity and density of a layer, the superscript + or - represents down-going or up-going propagation,  $z_m$  is the depth of the  $m^{\text{th}}$  interface in the  $z$  direction,  $p$  is an incoming wavefield,  $q$  is an outgoing wavefield,  $t$  or  $r$  is a transmission or reflection coefficient,  $s$  is an injection source wavefield, and  $w$  is a one-way propagator.

Figure 2: A 2-layer model to illustrate the concept of inverse propagation.

Figure 3: The true 1.5D model.

Figure 4: (a) The amplitude spectrum of the source wavefield in our simulation. (b) The source wavefield in the  $x$ - $t$  domain.

Figure 5. The measured surface wavefield when only considering internal multiples. The maximum multiple order is 10.

Figure 6. The situation when only internal multiples are considered and the maximum multiple order is 10. (Top left) The ground truth of the up-going and incoming wavefield  $p_n^-$  at  $z = 175 \text{ m}$ . (Top middle) The reconstructed up-going and incoming wavefield  $\tilde{p}_n^-$  at  $z = 175 \text{ m}$  via the inverse propagation of the surface wavefield  $p_n^-(0)$ . (Top right) The reconstructed up-going and incoming wavefield  $\tilde{p}_n^-$  at  $z = 175 \text{ m}$  via the backward propagation scheme used in the traditional JMI (OJMI). (Bottom left) The true 1.5D velocity with the red arrow pointing at the target subsurface interface. (Bottom middle) The

difference between the reconstructed wavefield via the inverse propagation and the ground truth. (Bottom right) The difference between the reconstructed wavefield via the backward propagation and the ground truth.

Figure 7. The situation when only internal multiples are considered and the maximum multiple order is 10. (Top left) The ground truth of the down-going and incoming wavefield  $p_n^+$  at  $z = 125 \text{ m}$ . (Top middle) The reconstructed down-going and incoming wavefield  $\widetilde{p}_n^+$  at  $z = 125 \text{ m}$  via the inverse propagation of the surface wavefield  $p_n^-(0)$ . (Top right) The reconstructed down-going and incoming wavefield  $\widetilde{p}_n^+$  at  $z = 125 \text{ m}$  via the backward propagation scheme used in the traditional JMI (OJMI). (Bottom left) The true 1.5D velocity with the red arrow pointing at the target subsurface interface. (Bottom middle) The difference between the reconstructed wavefield via the inverse propagation and the ground truth. (Bottom right) The difference between the reconstructed wavefield via the backward propagation and the ground truth.

Figure 8. The situation when only internal multiples are considered and the maximum multiple order is 10. (Top left) The ground truth of the down-going and outgoing wavefield  $q_{n-1}^+$  at  $z = 0 \text{ m}$ , the surface. (Top middle) The reconstructed down-going and incoming wavefield  $\widetilde{q}_{n-1}^+$  at  $z = 0 \text{ m}$  via the inverse propagation of the surface wavefield  $p_n^-(0)$ . (Top right) The reconstructed down-going and incoming wavefield  $\widetilde{q}_{n-1}^+$  at  $z = 0 \text{ m}$  via the backward propagation scheme used in the traditional JMI (OJMI). (Bottom left) The true 1.5D velocity with the red arrow pointing at the target subsurface interface. (Bottom middle) The difference between the reconstructed wavefield via the inverse propagation and the ground truth. (Bottom right) The difference between the reconstructed wavefield via the backward propagation and the ground truth.

Figure 9. The measured surface wavefield when considering both surface and internal multiples. The maximum multiple order is 5.

Figure 10. The situation when both surface and internal multiples are considered and the maximum multiple order is 5. (Top left) The ground truth of the up-going and incoming wavefield  $p_n^-$  at  $z = 175$  m. (Top middle) The reconstructed up-going and incoming wavefield  $\widetilde{p}_n^-$  at  $z = 175$  m via the inverse propagation of the surface wavefield  $p_n^-(0)$ . (Top right) The reconstructed up-going and incoming wavefield  $\widetilde{p}_n^-$  at  $z = 175$  m via the backward propagation scheme used in the traditional JMI (OJMI). (Bottom left) The true 1.5D velocity with the red arrow pointing at the target subsurface interface. (Bottom middle) The difference between the reconstructed wavefield via the inverse propagation and the ground truth. (Bottom right) The difference between the reconstructed wavefield via the backward propagation and the ground truth.

Figure 11. The situation when both surface and internal multiples are considered and the maximum multiple order is 5. (Top left) The ground truth of the down-going and incoming wavefield  $p_n^+$  at  $z = 125$  m. (Top middle) The reconstructed down-going and incoming wavefield  $\widetilde{p}_n^+$  at  $z = 125$  m via the inverse propagation of the surface wavefield  $p_n^-(0)$ . (Top right) The reconstructed down-going and incoming wavefield  $\widetilde{p}_n^+$  at  $z = 125$  m via the backward propagation scheme used in the traditional JMI (OJMI). (Bottom left) The true 1.5D velocity with the red arrow pointing at the target subsurface interface. (Bottom middle) The difference between the reconstructed wavefield via the inverse propagation and the ground truth. (Bottom right) The difference between the reconstructed wavefield via the backward propagation and the ground truth.

Figure 12. The situation when both surface and internal multiples are considered and the maximum multiple order is 5. (Top left) The ground truth of the down-going and outgoing wavefield  $q_{n-1}^+$  at  $z =$

0 m, the surface. (Top middle) The reconstructed down-going and incoming wavefield  $\widetilde{q_{n-1}^+}$  at  $z = 0$  m via the inverse propagation of the surface wavefield  $p_n^-(0)$ . (Top right) The reconstructed down-going and incoming wavefield  $\widetilde{q_{n-1}^+}$  at  $z = 0$  m via the backward propagation scheme used in the traditional JMI (OJMI). (Bottom left) The true 1.5D velocity with the red arrow pointing at the target subsurface interface. (Bottom middle) The difference between the reconstructed wavefield via the inverse propagation and the ground truth. (Bottom right) The difference between the reconstructed wavefield via the backward propagation and the ground truth.

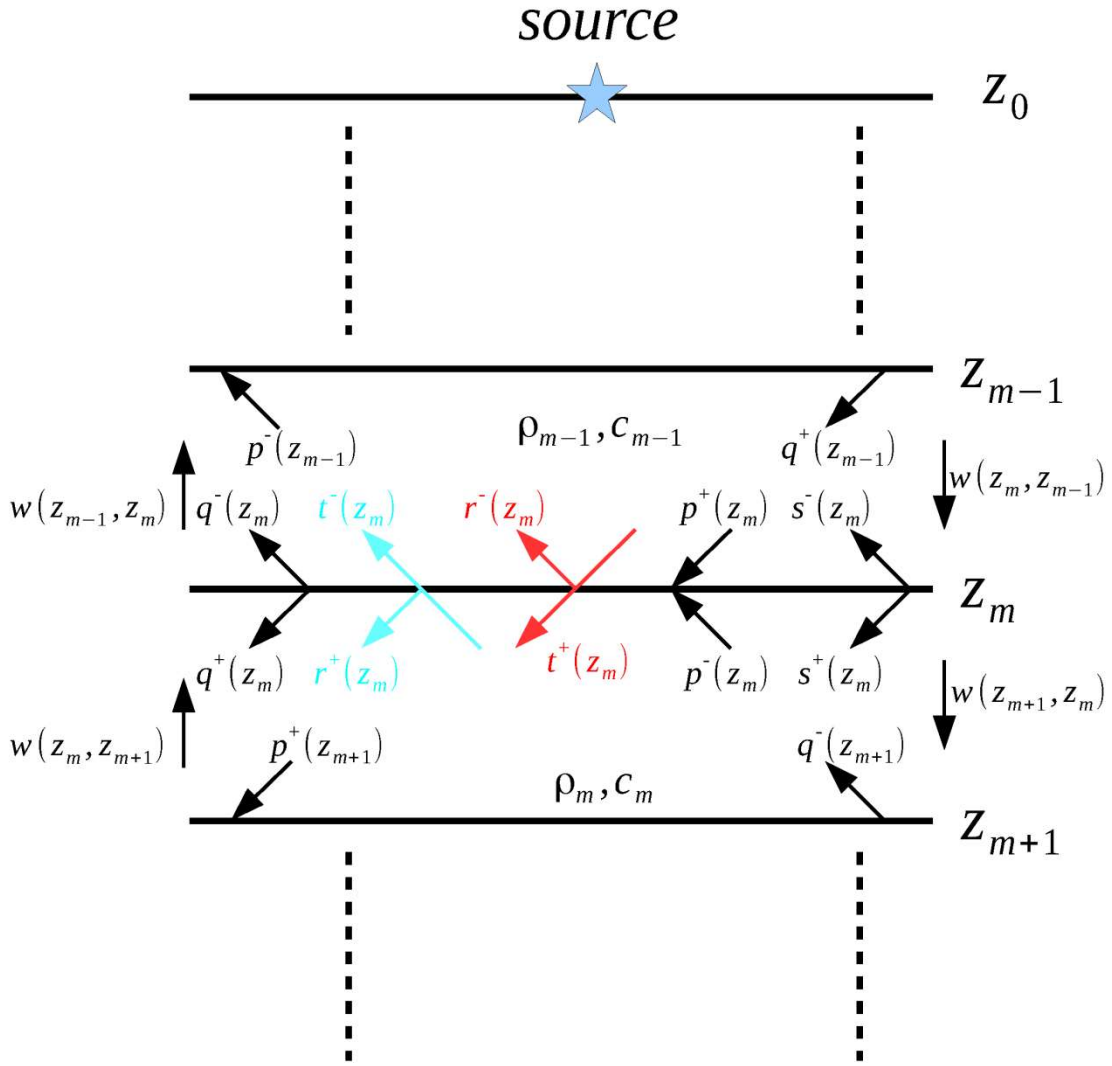


Figure 1: The fundamental wavefield propagation model used in 1.5D-AVO-FWMod and 1.5D-AVO-JMI. Note that all the wavefield-related symbols in this figure are actually subject to a certain combination of  $k_x$  and  $\omega$ . For example,  $q^+(z_m)$  there actually represents  $q^+(z_m; k_x, \omega)$ . The symbols shown in this figure are defined as follows:  $\rho$  and  $c$  are velocity and density of a layer, the superscript + or - represents down-going or up-going propagation,  $z_m$  is the depth of the  $m^{\text{th}}$  interface in the  $z$  direction,  $p$  is an incoming wavefield,  $q$  is an outgoing wavefield,  $t$  or  $r$  is a transmission or reflection coefficient,  $s$  is an injection source wavefield, and  $w$  is a one-way propagator.

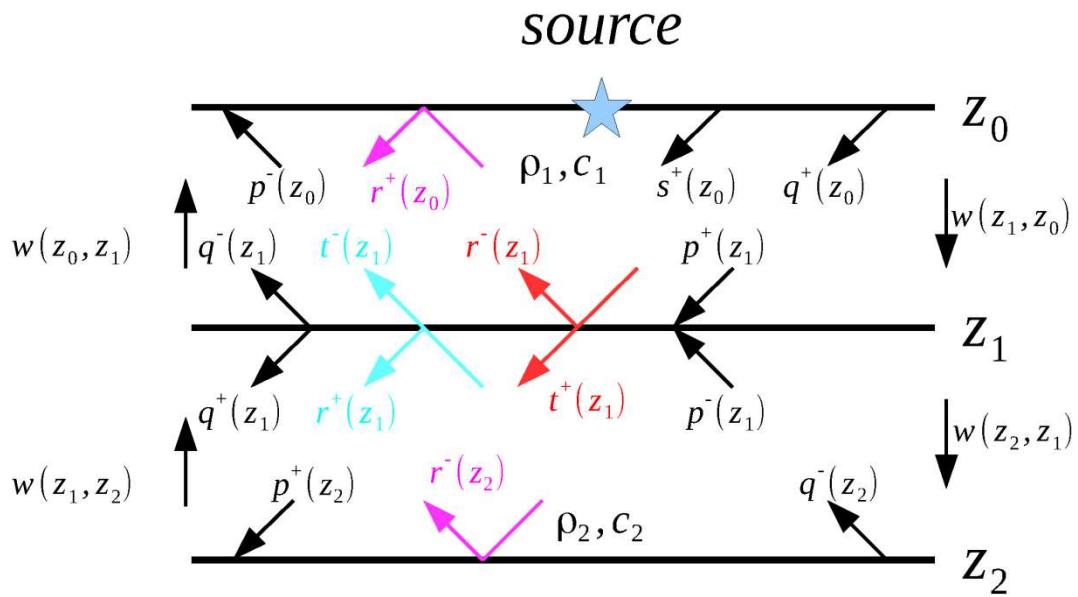


Figure 2: A 2-layer model to illustrate the concept of inverse propagation.

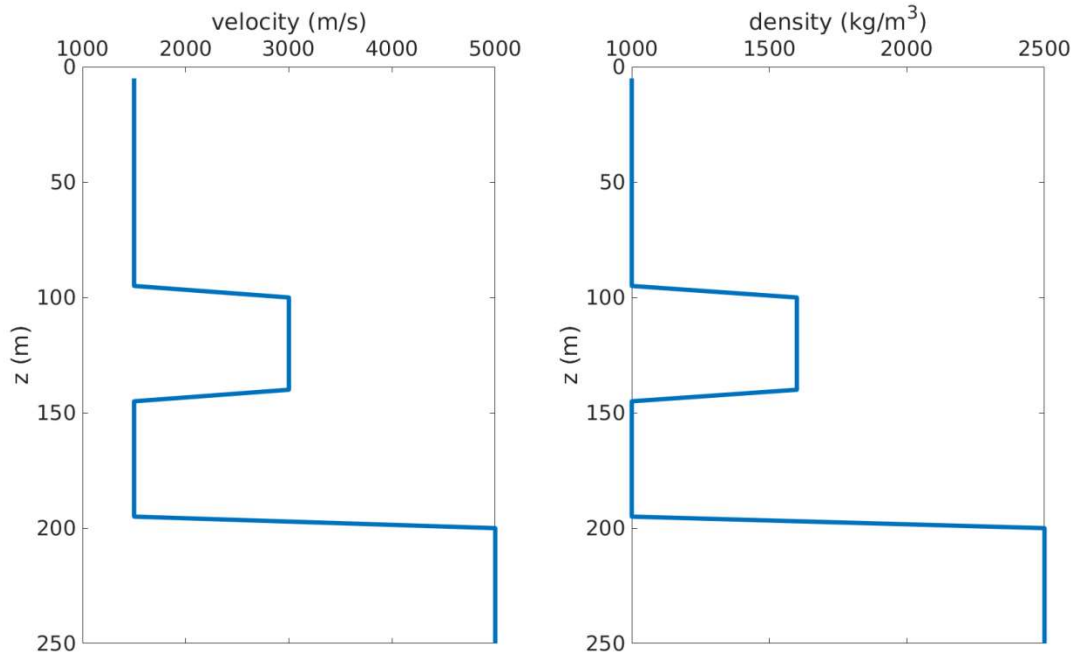
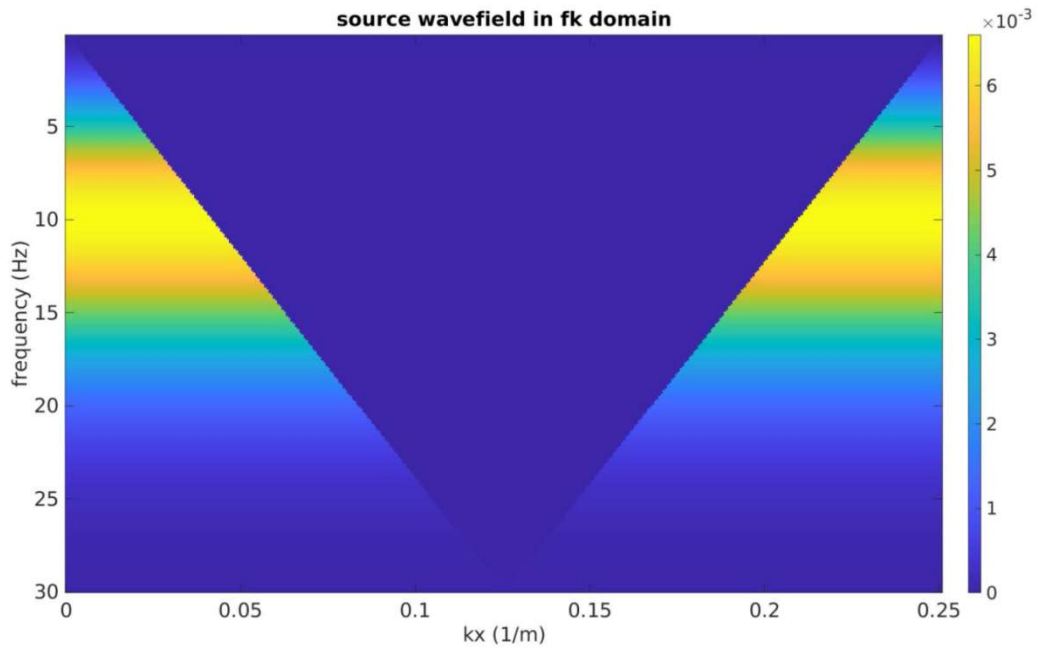
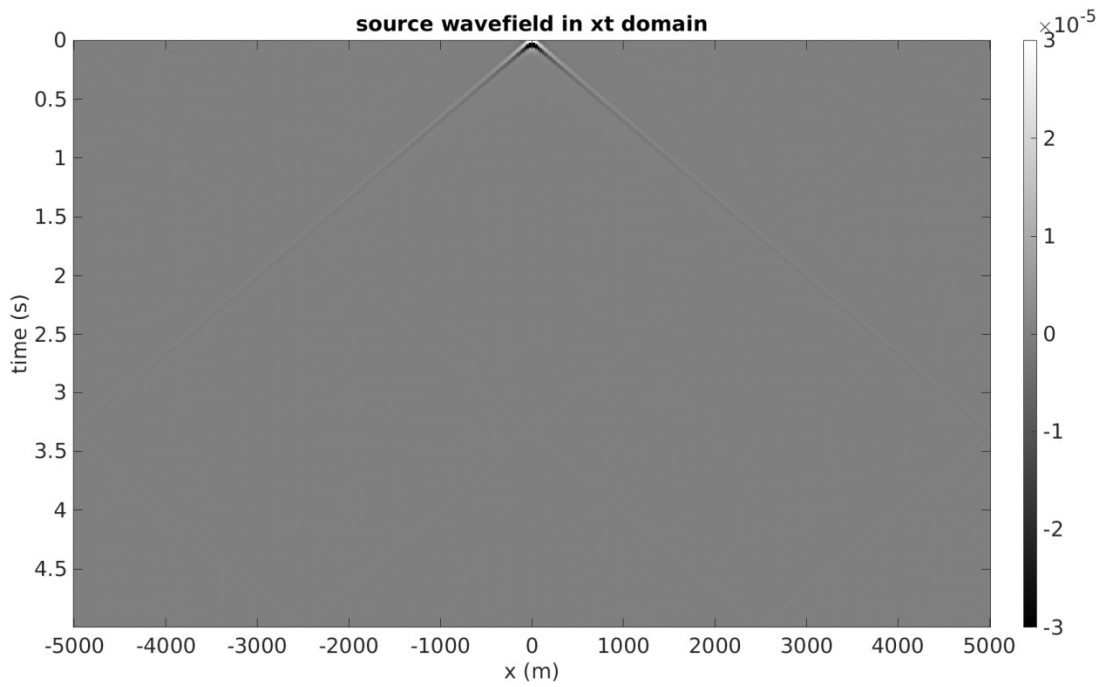


Figure 3: The true 1.5D model.



(a)



(b)

Figure 4: (a) The amplitude spectrum of the source wavefield in our simulation. (b) The source wavefield in the  $x-t$  domain.

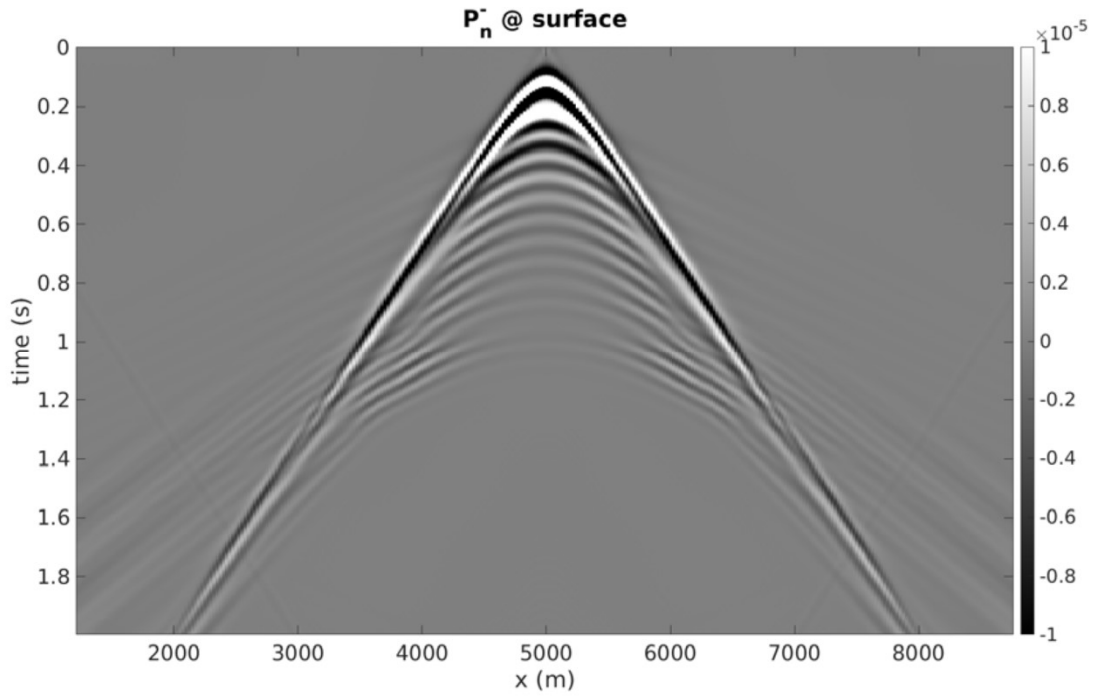


Figure 5. The measured surface wavefield when only considering internal multiples. The maximum multiple order is 10.

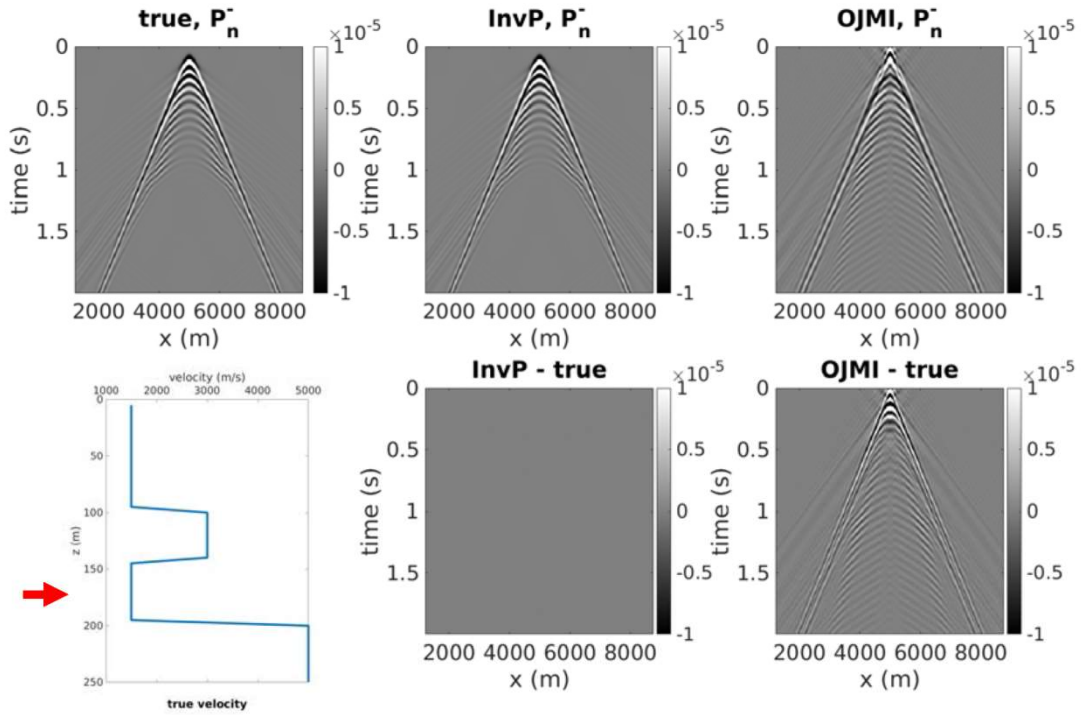


Figure 6. The situation when only internal multiples are considered and the maximum multiple order is 10. (Top left) The ground truth of the up-going and incoming wavefield  $p_n^-$  at  $z = 175$  m. (Top middle) The reconstructed up-going and incoming wavefield  $\tilde{p}_n^-$  at  $z = 175$  m via the inverse propagation of the surface wavefield  $p_n^-(0)$ . (Top right) The reconstructed up-going and incoming wavefield  $\tilde{p}_n^-$  at  $z = 175$  m via the backward propagation scheme used in the traditional JMI (OJMI). (Bottom left) The true 1.5D velocity with the red arrow pointing at the target subsurface interface. (Bottom middle) The difference between the reconstructed wavefield via the inverse propagation and the ground truth. (Bottom right) The difference between the reconstructed wavefield via the backward propagation and the ground truth.

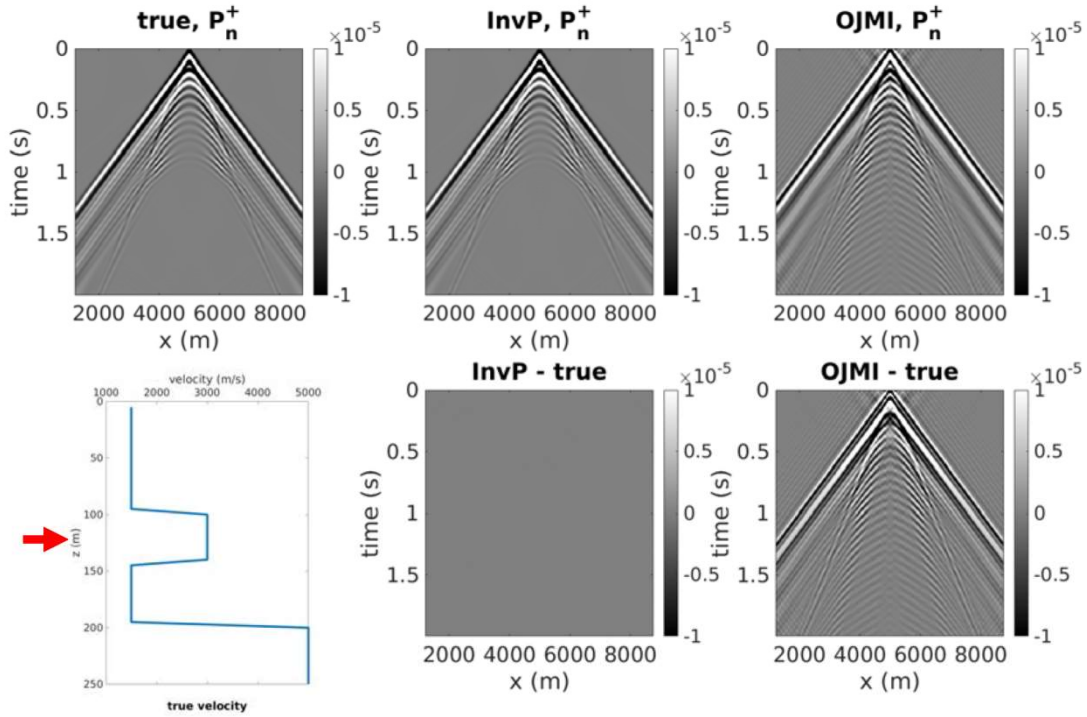


Figure 7. The situation when only internal multiples are considered and the maximum multiple order is 10. (Top left) The ground truth of the down-going and incoming wavefield  $p_n^+$  at  $z = 125$  m. (Top middle) The reconstructed down-going and incoming wavefield  $\widetilde{p}_n^+$  at  $z = 125$  m via the inverse propagation of the surface wavefield  $p_n^-(0)$ . (Top right) The reconstructed down-going and incoming wavefield  $\widetilde{p}_n^+$  at  $z = 125$  m via the backward propagation scheme used in the traditional JMI (OJMI). (Bottom left) The true 1.5D velocity with the red arrow pointing at the target subsurface interface. (Bottom middle) The difference between the reconstructed wavefield via the inverse propagation and the ground truth. (Bottom right) The difference between the reconstructed wavefield via the backward propagation and the ground truth.

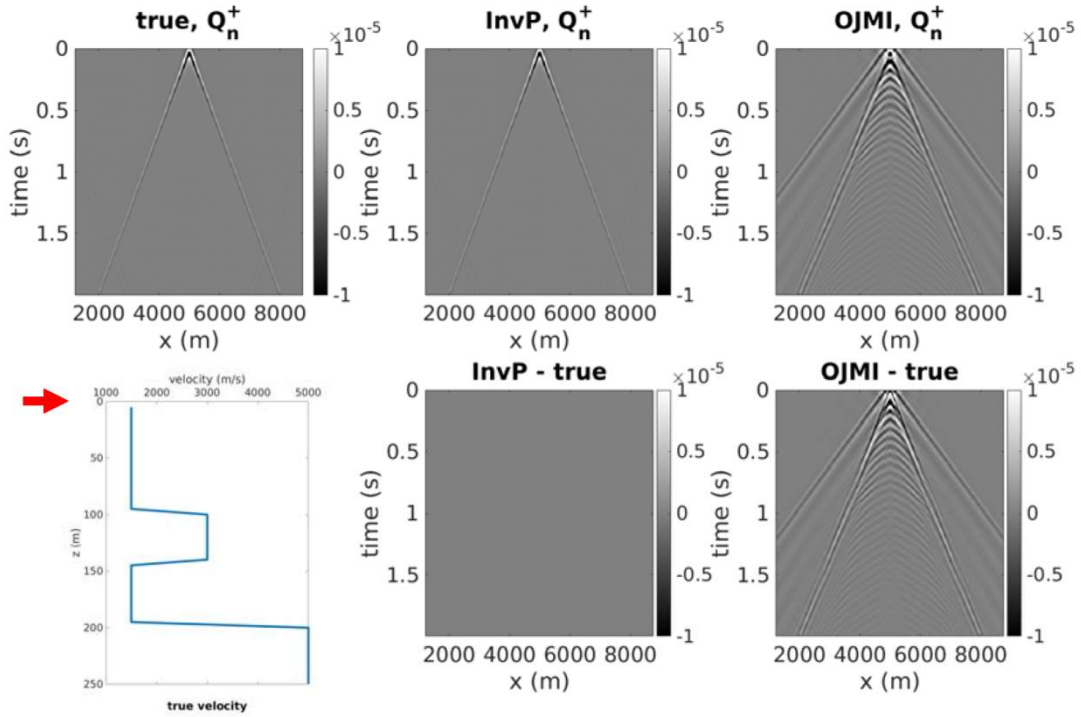


Figure 8. The situation when only internal multiples are considered and the maximum multiple order is 10. (Top left) The ground truth of the down-going and outgoing wavefield  $q_{n-1}^+$  at  $z = 0$  m, the surface. (Top middle) The reconstructed down-going and incoming wavefield  $\widetilde{q}_{n-1}^+$  at  $z = 0$  m via the inverse propagation of the surface wavefield  $p_n^-(0)$ . (Top right) The reconstructed down-going and incoming wavefield  $\widetilde{q}_{n-1}^+$  at  $z = 0$  m via the backward propagation scheme used in the traditional JMI (OJMI). (Bottom left) The true 1.5D velocity with the red arrow pointing at the target subsurface interface. (Bottom middle) The difference between the reconstructed wavefield via the inverse propagation and the ground truth. (Bottom right) The difference between the reconstructed wavefield via the backward propagation and the ground truth.

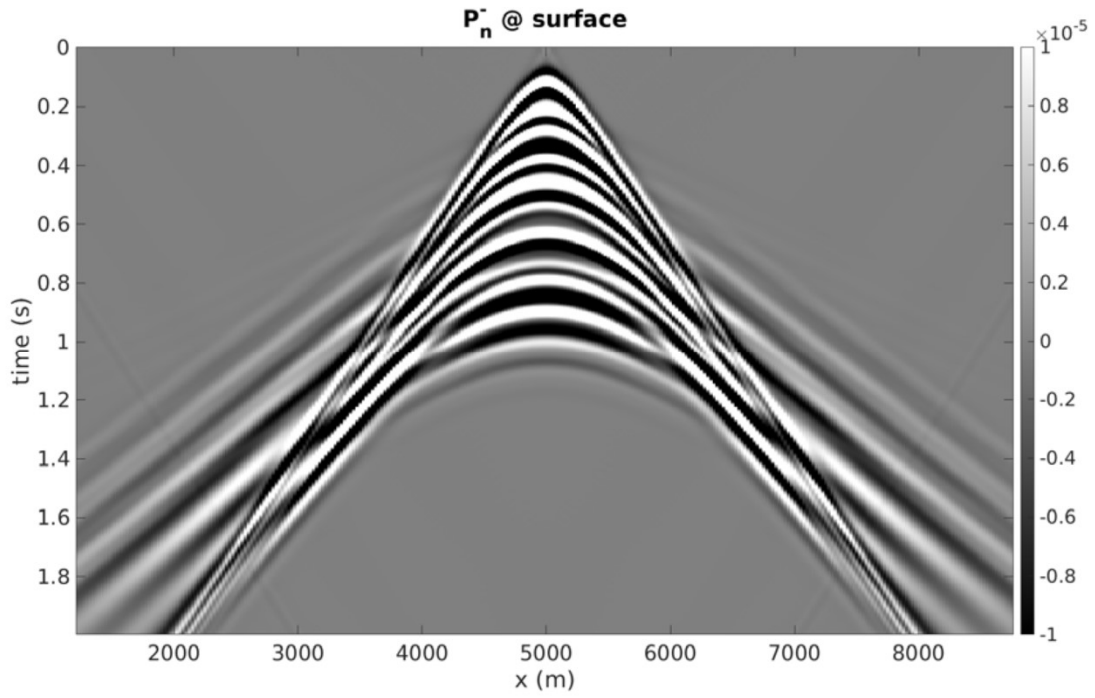


Figure 9. The measured surface wavefield when considering both surface and internal multiples. The maximum multiple order is 5.

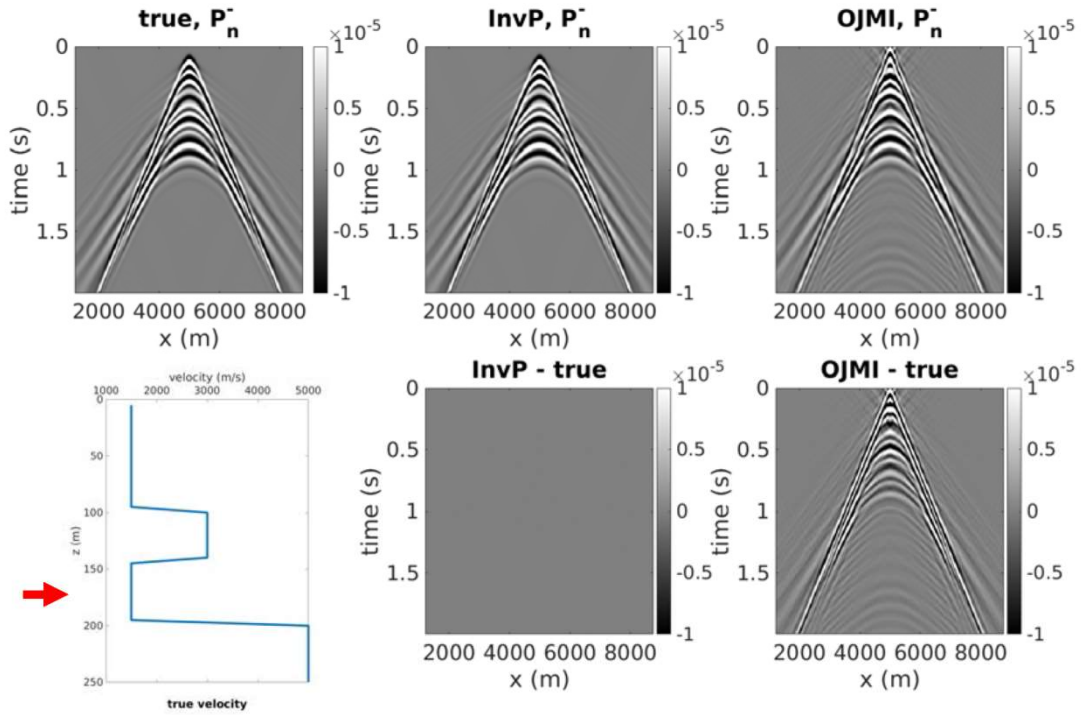


Figure 10. The situation when both surface and internal multiples are considered and the maximum multiple order is 5. (Top left) The ground truth of the up-going and incoming wavefield  $p_n^-$  at  $z = 175$  m. (Top middle) The reconstructed up-going and incoming wavefield  $\tilde{p}_n^-$  at  $z = 175$  m via the inverse propagation of the surface wavefield  $p_n^-(0)$ . (Top right) The reconstructed up-going and incoming wavefield  $\tilde{p}_n^-$  at  $z = 175$  m via the backward propagation scheme used in the traditional JMI (OJMI). (Bottom left) The true 1.5D velocity with the red arrow pointing at the target subsurface interface. (Bottom middle) The difference between the reconstructed wavefield via the inverse propagation and the ground truth. (Bottom right) The difference between the reconstructed wavefield via the backward propagation and the ground truth.

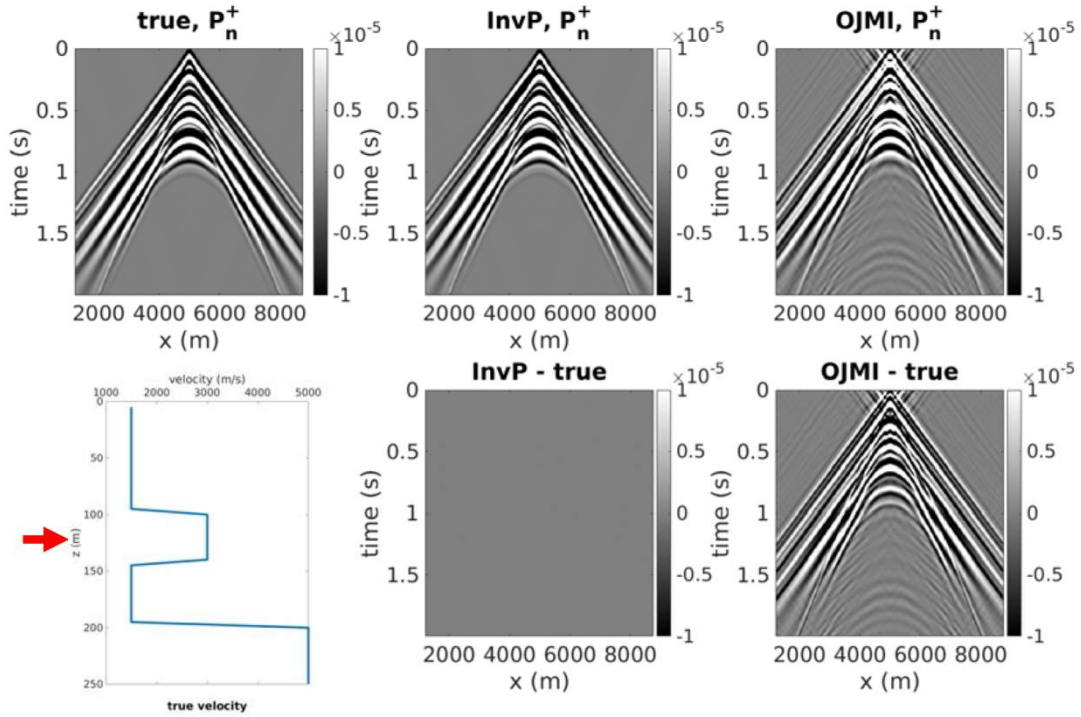


Figure 11. The situation when both surface and internal multiples are considered and the maximum multiple order is 5. (Top left) The ground truth of the down-going and incoming wavefield  $p_n^+$  at  $z = 125$  m. (Top middle) The reconstructed down-going and incoming wavefield  $\widetilde{p}_n^+$  at  $z = 125$  m via the inverse propagation of the surface wavefield  $p_n^-(0)$ . (Top right) The reconstructed down-going and incoming wavefield  $\widetilde{p}_n^+$  at  $z = 125$  m via the backward propagation scheme used in the traditional JMI (OJMI). (Bottom left) The true 1.5D velocity with the red arrow pointing at the target subsurface interface. (Bottom middle) The difference between the reconstructed wavefield via the inverse propagation and the ground truth. (Bottom right) The difference between the reconstructed wavefield via the backward propagation and the ground truth.

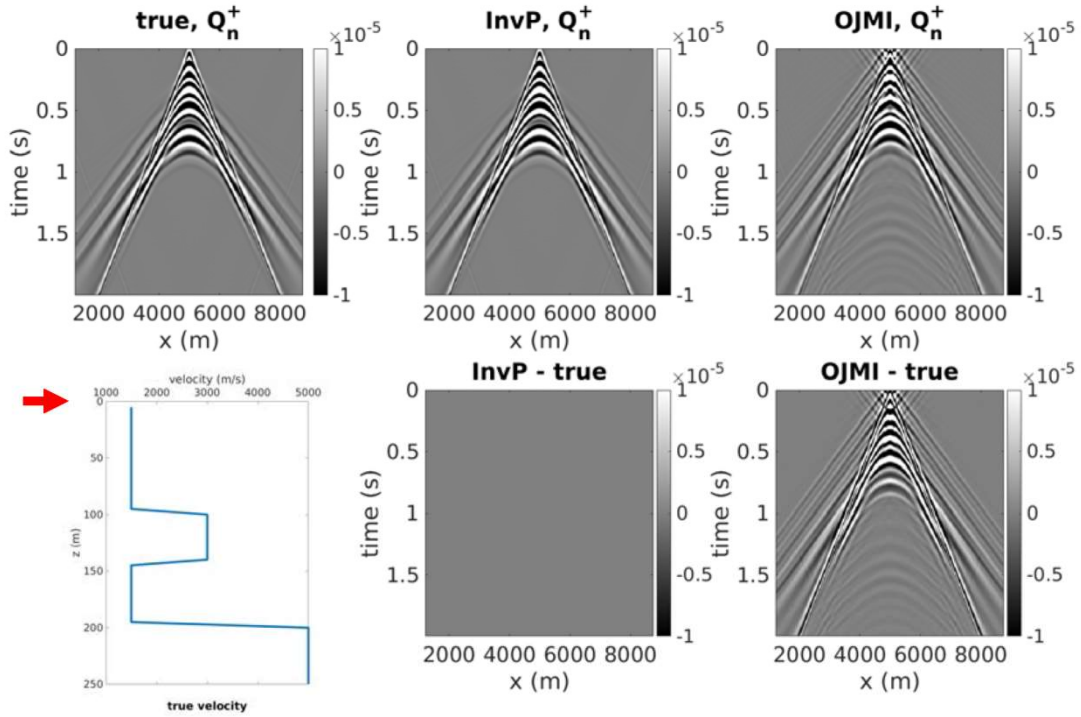


Figure 12. The situation when both surface and internal multiples are considered and the maximum multiple order is 5. (Top left) The ground truth of the down-going and outgoing wavefield  $q_n^+$  at  $z = 0$  m, the surface. (Top middle) The reconstructed down-going and incoming wavefield  $\widetilde{q_{n-1}^+}$  at  $z = 0$  m via the inverse propagation of the surface wavefield  $p_n^-(0)$ . (Top right) The reconstructed down-going and incoming wavefield  $\widetilde{q_{n-1}^+}$  at  $z = 0$  m via the backward propagation scheme used in the traditional JMI (OJMI). (Bottom left) The true 1.5D velocity with the red arrow pointing at the target subsurface interface. (Bottom middle) The difference between the reconstructed wavefield via the inverse propagation and the ground truth. (Bottom right) The difference between the reconstructed wavefield via the backward propagation and the ground truth.